S1 Expansion to empirical and modelled results

Intensity values are not directly comparable between plots as data is un-calibrated. Drops to zero intensity represent regions where impurity content was below what is detectable.

Plots for EDC LGP

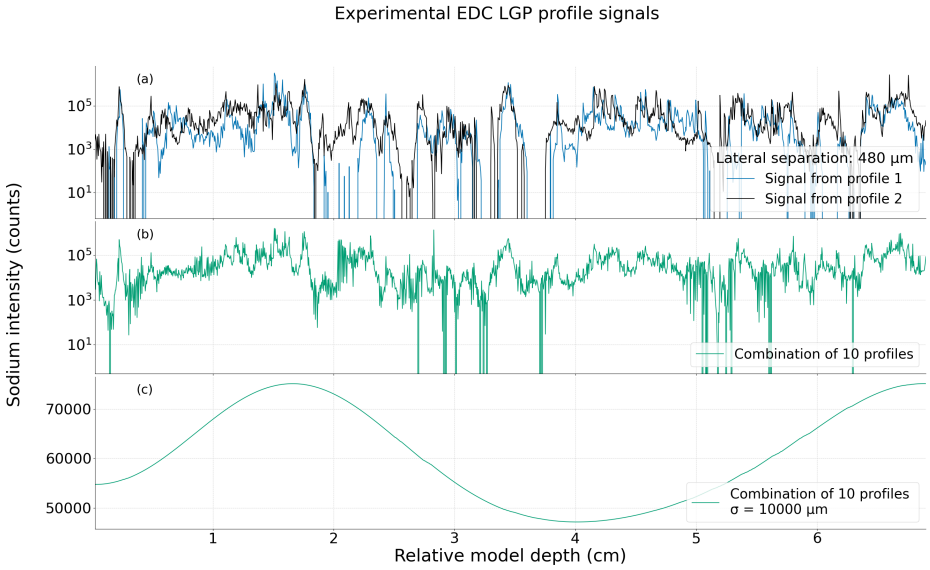

Figure S1. Measured LA-ICP-MS signals resulting from line profiles taken across the surface of the EDC LGP. All profiles run down the central core axis. Panel (a) shows two signals resulting from two parallel laser tracks. Panel (b) shows the spatially averaged signal resulting from combining all measured parallel profiles, including the two signals in (a), with a range of separations between adjacent profiles. Panel (c) shows this spatially averaged signal after smoothing to CFA-resolution of 1 cm.

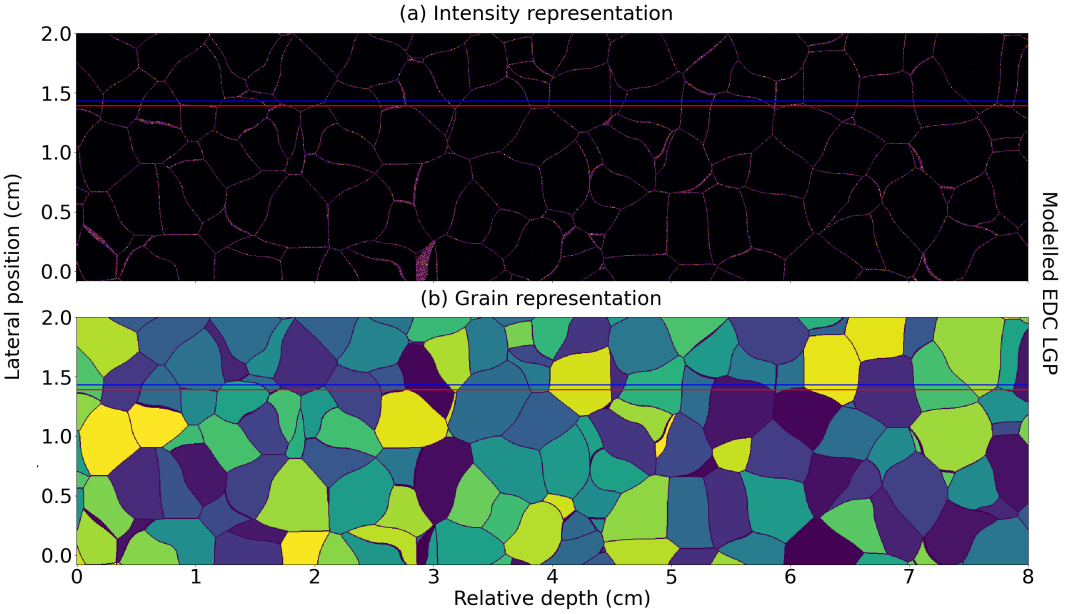

Figure S2. The intensity, (a), and structural, (b), representations of one modelled face of the EDC LGP sample. The structural representation shows grains as different colours, separated by grain boundaries represented in black. Each of the 500 rows in the intensity representation can be taken as a separate laser profile. The red and blue lines in both panels show the track of the profiles plotted in Fig. S3.

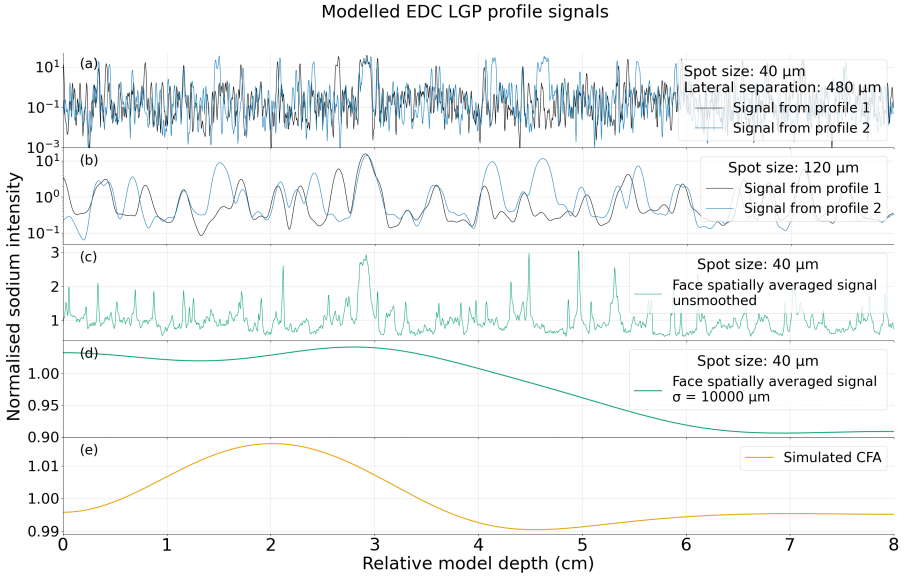

Figure S3. Line profile signals for the modelled EDC Holocene ice normalised by dividing by the volume average intensity. Panel (a) shows signals acquired from 40 μm spot size profiles taken from the tracks indicated in Fig. S2. Signals resulting from simulating a 120 μm spot size along these profiles are shown in (b). The resulting signal from combining all possible profiles from the face in Fig. S2 is shown unsmoothed in (c) and smoothed to CFA resolution in (d). The simulated CFA signal is plotted in (e). Note the different y-axis scales for each panel.

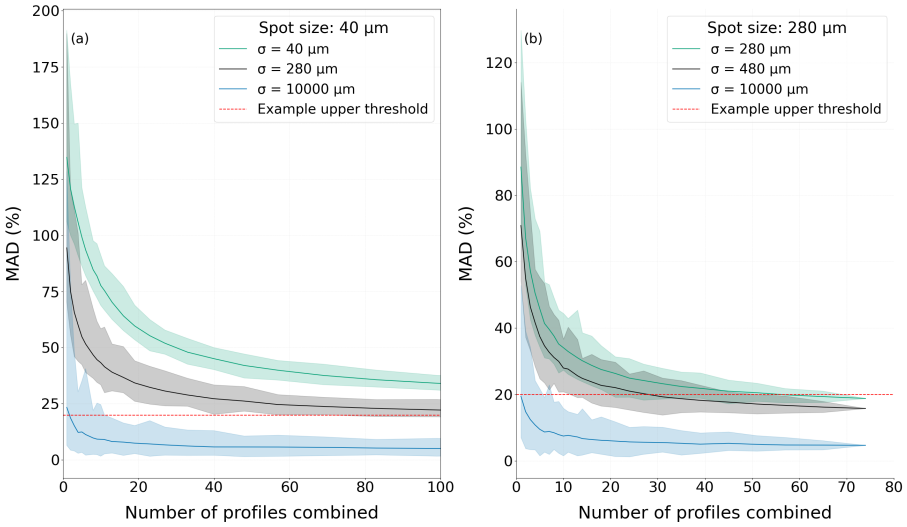

Figure S4. Plots of calculated MAD values against the number of LA-ICP-MS profiles used to construct a spatially averaged signal for the modelled EDC LGP face shown in Fig.S2. As there are multiple ways to choose profiles for combination into a spatially averaged signal, the solid line of each colour shows the mean result and the shaded region shows the range of MADs acquired for different possible combined profiles. Panels (a) and (c) show results from simulating a 40 μm laser spot and (b) and (d) a 280 μm laser spot. Different coloured regions show MAD values resulting from smoothing with different width Gaussian kernels. An arbitrary threshold of 20 % is also shown (red line).

Plots for RECAP Holocene

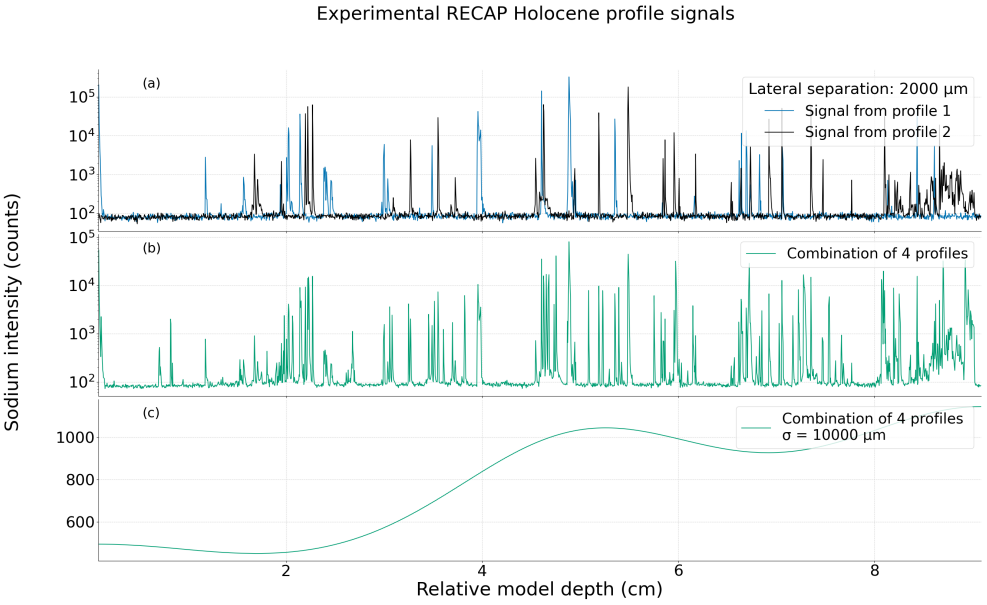

Figure S5. Plots equivalent to Fig. S1 showing the modelled data for RECAP Holocene

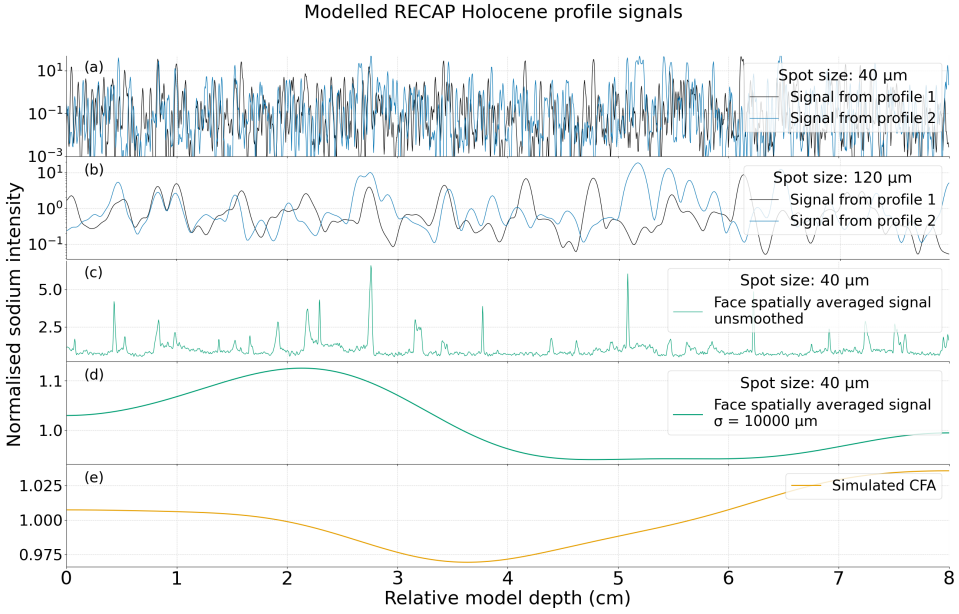

Figure S6. Plots equivalent to Fig. S3 for modelled RECAP Holocene

Plots for RECAP LGP

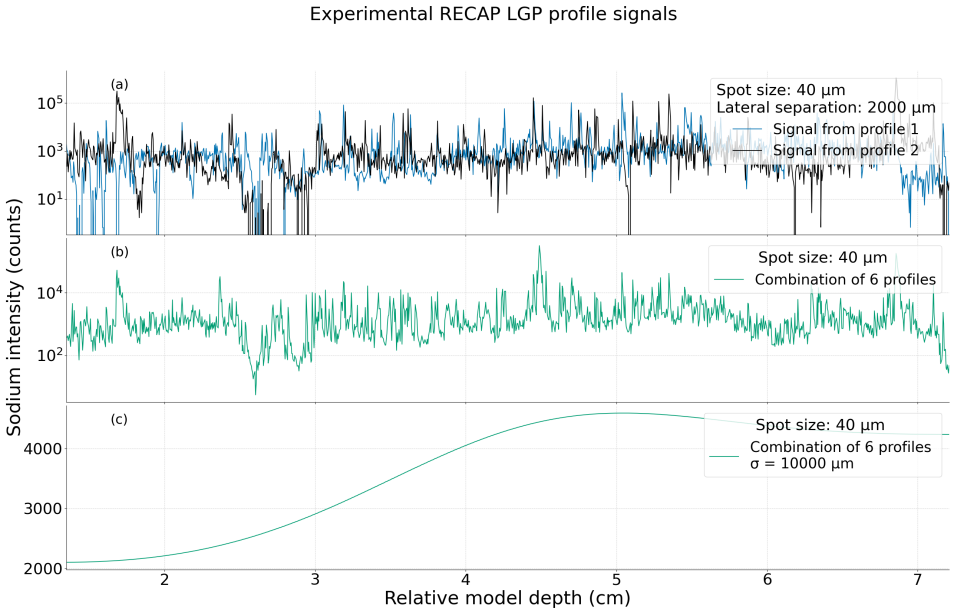

Figure S7. Plots equivalent to Fig. S1 showing the modelled data for RECAP LGP

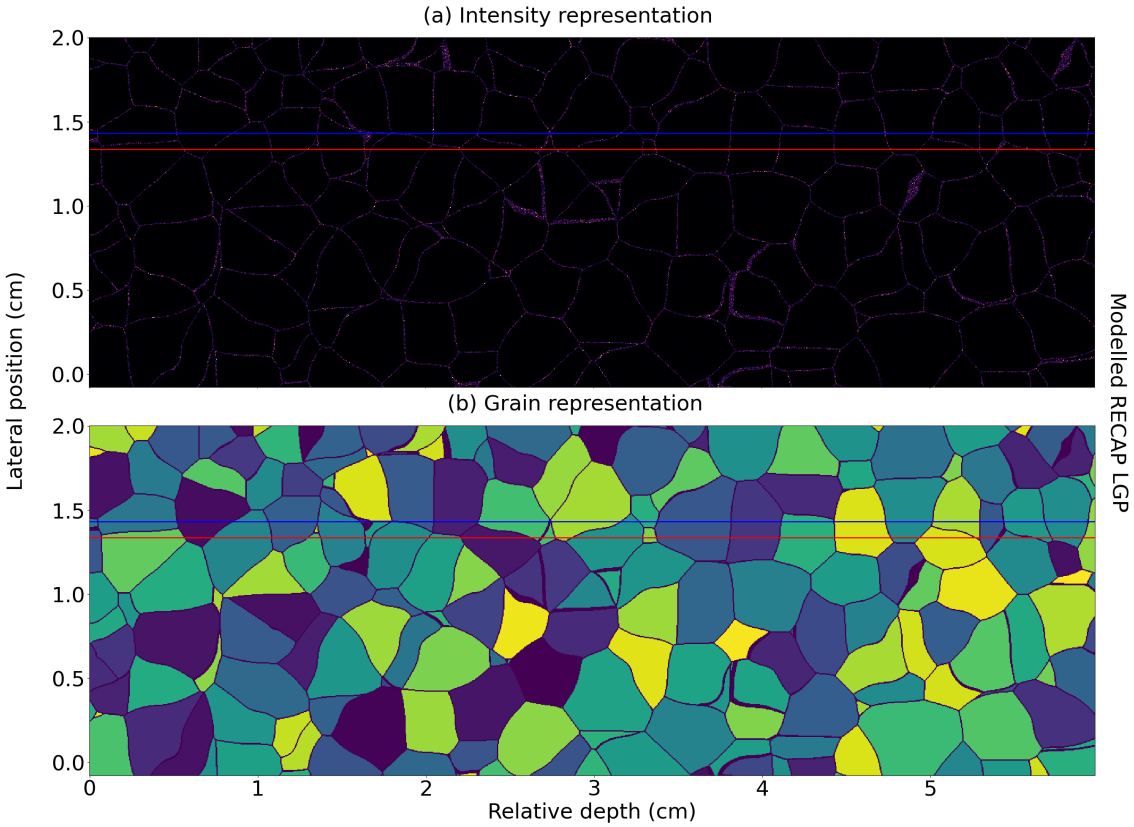

Figure S8. Plots equivalent to Fig. S2 showing the modelled data for RECAP LGP

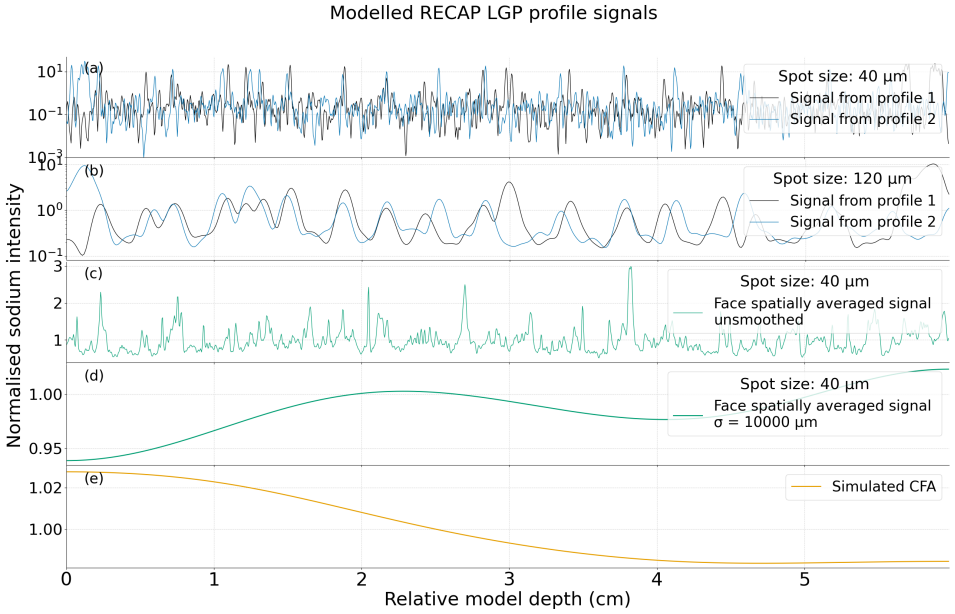

Figure S9. Plots equivalent to Fig. S3 showing the two profiles plotted in Fig. S8 for modelled RECAP LGP

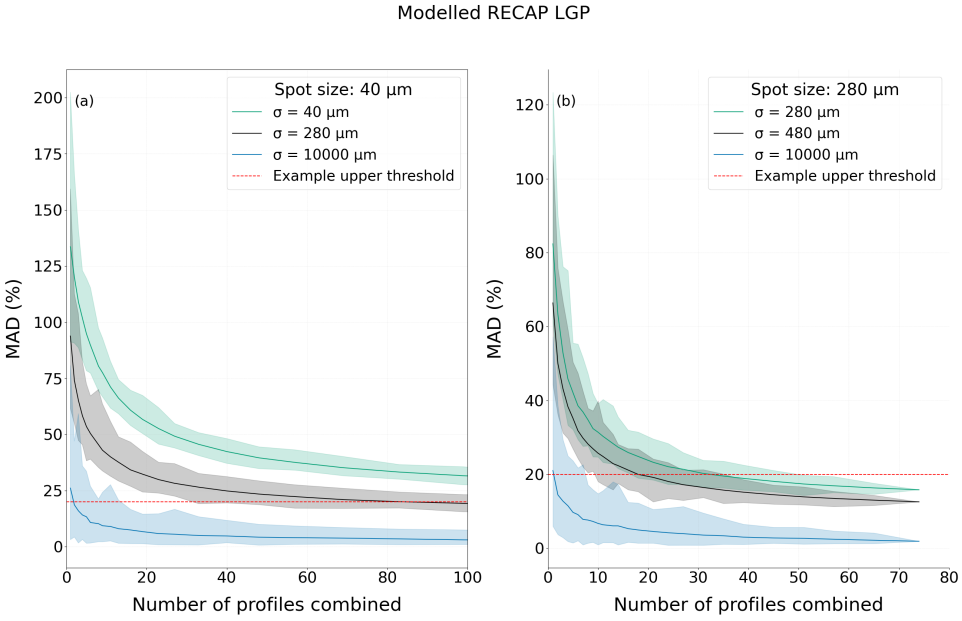

Figure S10. Plots equivalent to Fig. S4 for modelled RECAP LGM

S2 Grain volumes

The three-dimensional Poisson Voronoi tessellations used for this analysis are parameterised by the grain number density that matches the ice samples they represent. This number density, n, is calculated for ice samples as

$$n = \frac{1}{\frac{4}{3}\pi\bar{r}^3} \tag{S1}$$

for a sample with grains of mean radius $\bar{r}$, assuming spherical grain volume. The grain number density from equation S1 can be multiplied by the total volume of a modelled space, V,

$$N = Vn \tag{S2}$$

to get the total number of seed points, N, required to produce grains with mean size matching the target ice samples. Generating a Poisson Voronoi tessellation with a number of seeds set by equation S2 results in a modelled space that contains grains of varying volumes, v_i, with a mean grain volume $\bar{v}$,

$$\bar{v} = \frac{1}{N}\sum_{i=1}^{N} v_i. \tag{S3}$$

From this mean grain volume, a normalised grain volume y can be defined as

$$y = \frac{v}{\bar{v}} \tag{S4}$$

in which grains vary in size around conforming to a gamma distribution (Ferenc and Néda, 2007)

$$f(y) = \frac{3125}{24}(y)^4 \exp(-5y) \tag{S5}$$

which is plotted in figures S11, S13, and S14 alongside modelled grain size distributions.

Fig. S11 shows that modelled systems' grain volumes match the theoretical distribution, except for a shift to slightly smaller grain volumes than targeted and a large number of grains with very small volumes. This change in distribution can be explained by considering that, for all modelled ice samples, the ratio of the mean grain radius to the modelled volume size results in grains that only exist partially within the modelled space and that grain size measurements often discard very small grains. Typically, grain size analysis will be carried out only considering the Voronoi cells (grains) that are wholly contained in the modelled volume (Quey et al., 2011). Therefore, to truly extract the grain volume distribution, a sufficient number of grains must exist wholly within the simulated volume, which is not the case for samples modelled in this study.

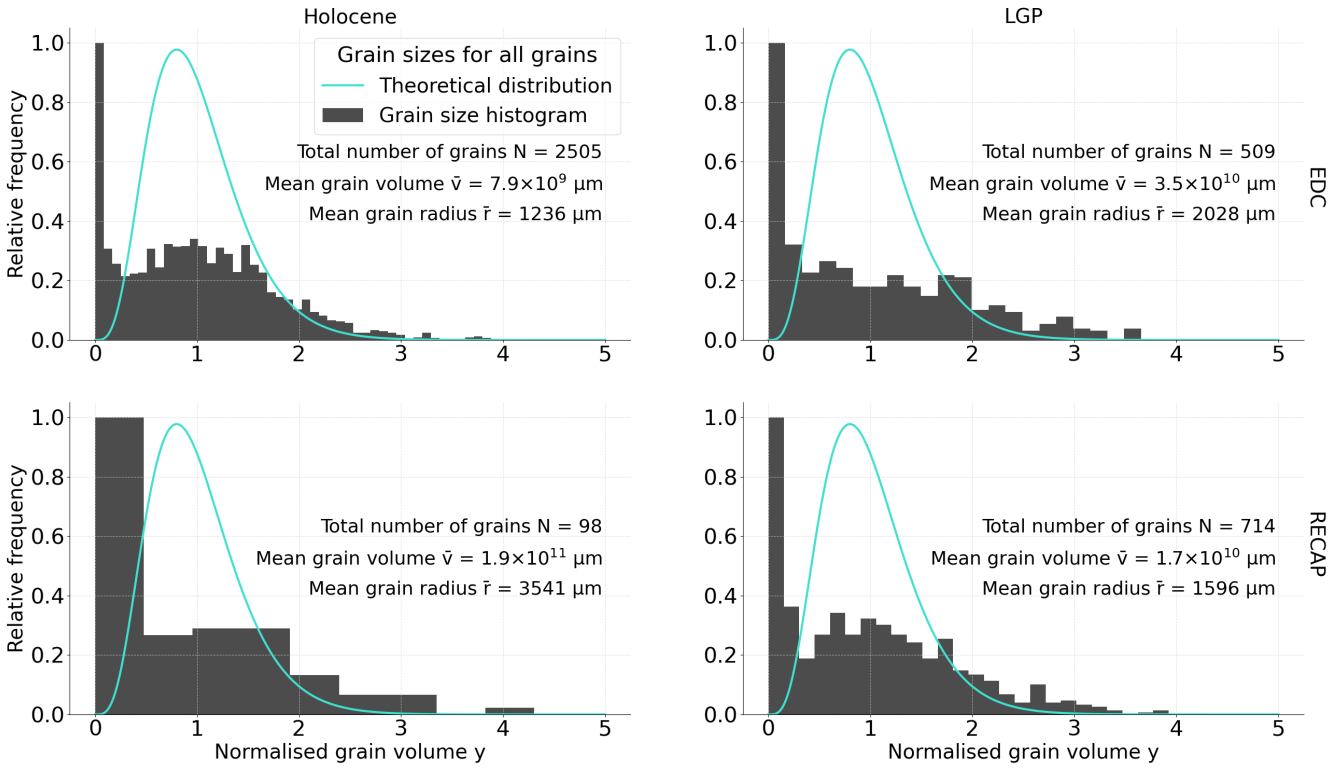

Figure S11. Grain volume distribution for all modelled samples. Bin widths differ due to the different total numbers of grains.

To explore the statistics of grain volumes generated by the Voronoi tessellation used in this study, a model which has a large number of grains wholly within its volume was produced. This modelled volume, shown partially in Fig. S12, has a relatively large cubic volume, with voxel dimension $40\,\mu\mathrm{m}$, volume side length $12\,000\,\mu\mathrm{m}$, and a relatively small target grain radius of $400\,\mu\mathrm{m}$. This modelled volume does not represent any specific real ice sample. Fig. S13 shows the grain volume distribution for all grains in this space, calculated by counting the number of voxels in each grain. Fig. S14 shows the subset of grains, only 15% of the total, in this volume that are wholly contained. The grains contained wholly in the volume have an average grain volume of $410\,\mu\mathrm{m}$ and conform well to the expected grain volume distribution reported in equation S5.

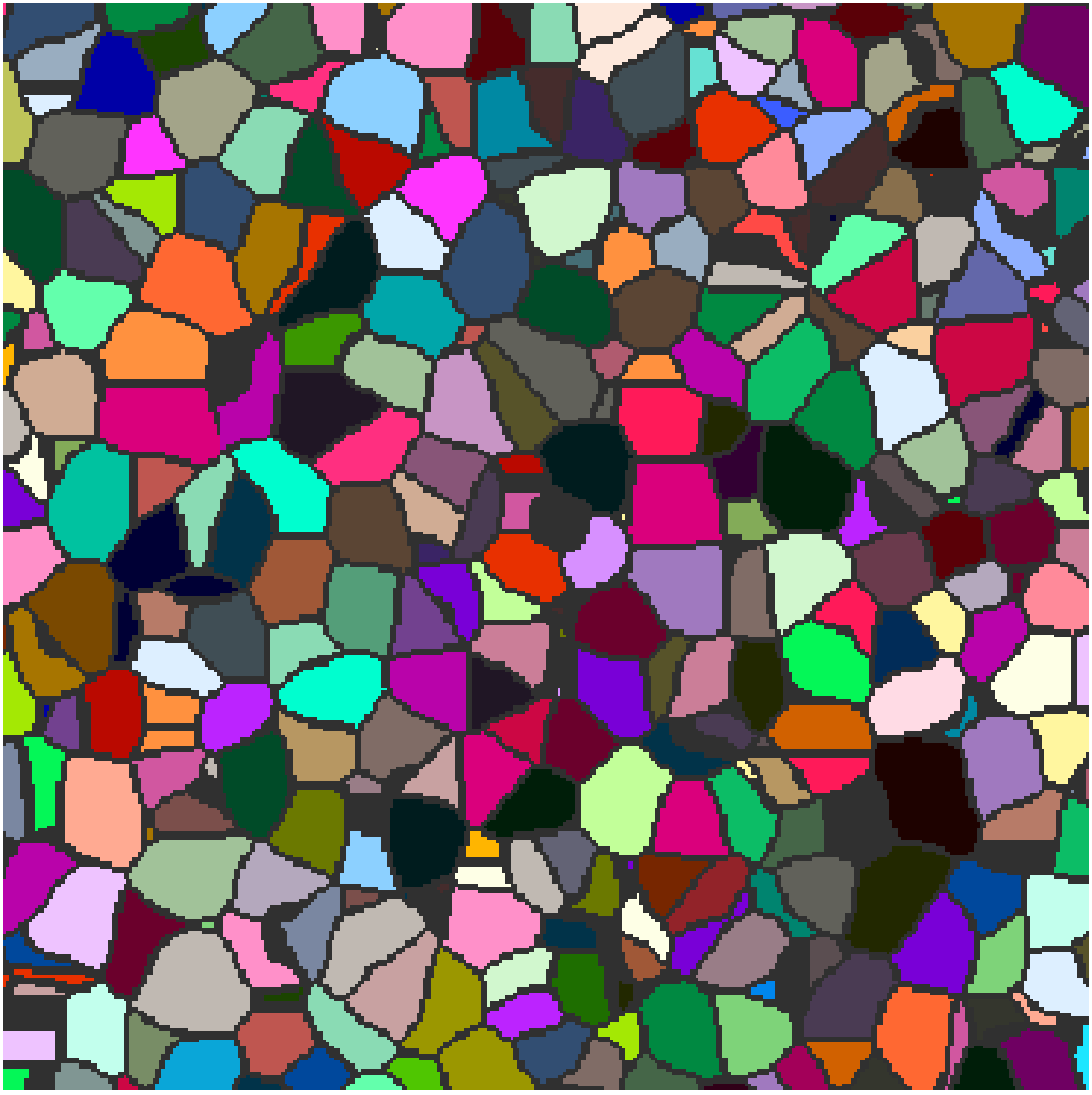

Figure S12. Two-dimensional representation of a face of a cube, dimension 12 000 µm, with grains resulting from a Poisson Voronoi tessellation shown in different colours and the boundaries between these grains shown in grey.

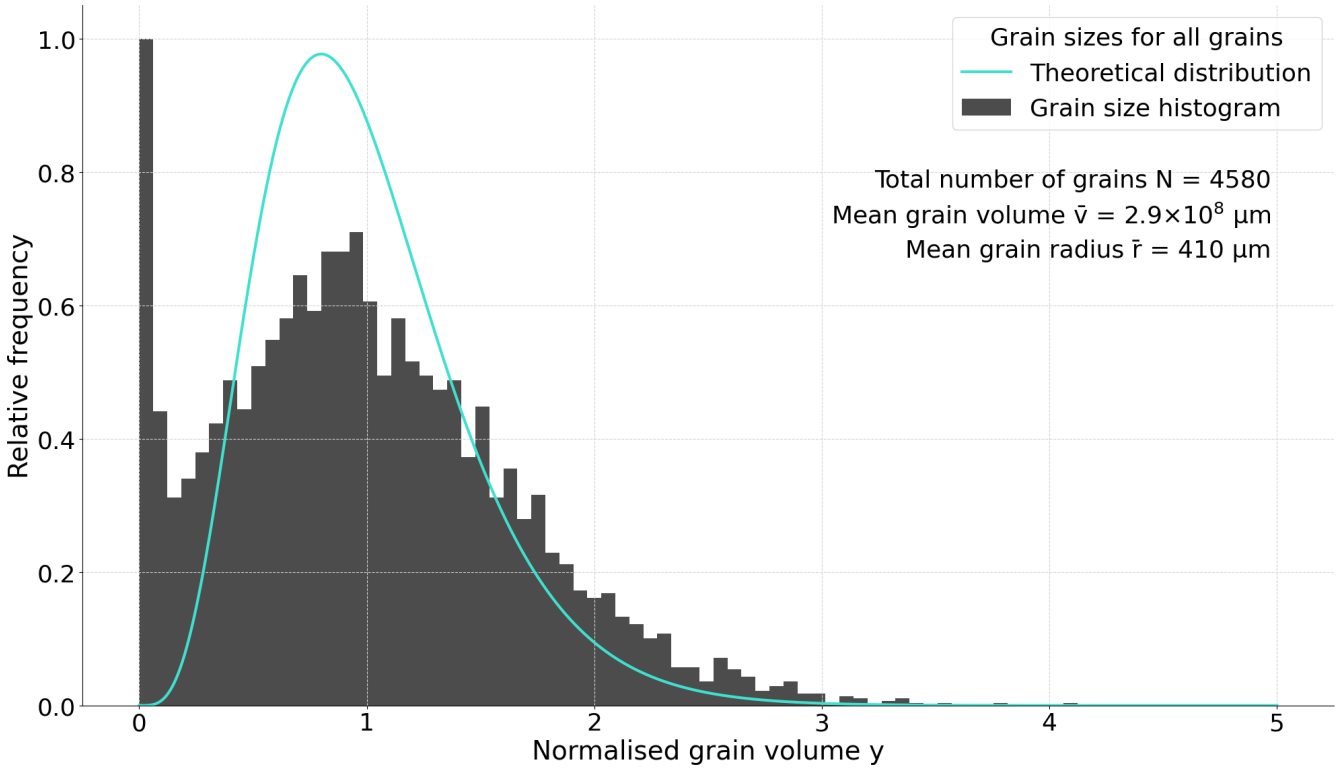

Figure S13. Grain volume distribution for all grains generated in Fig. S12.

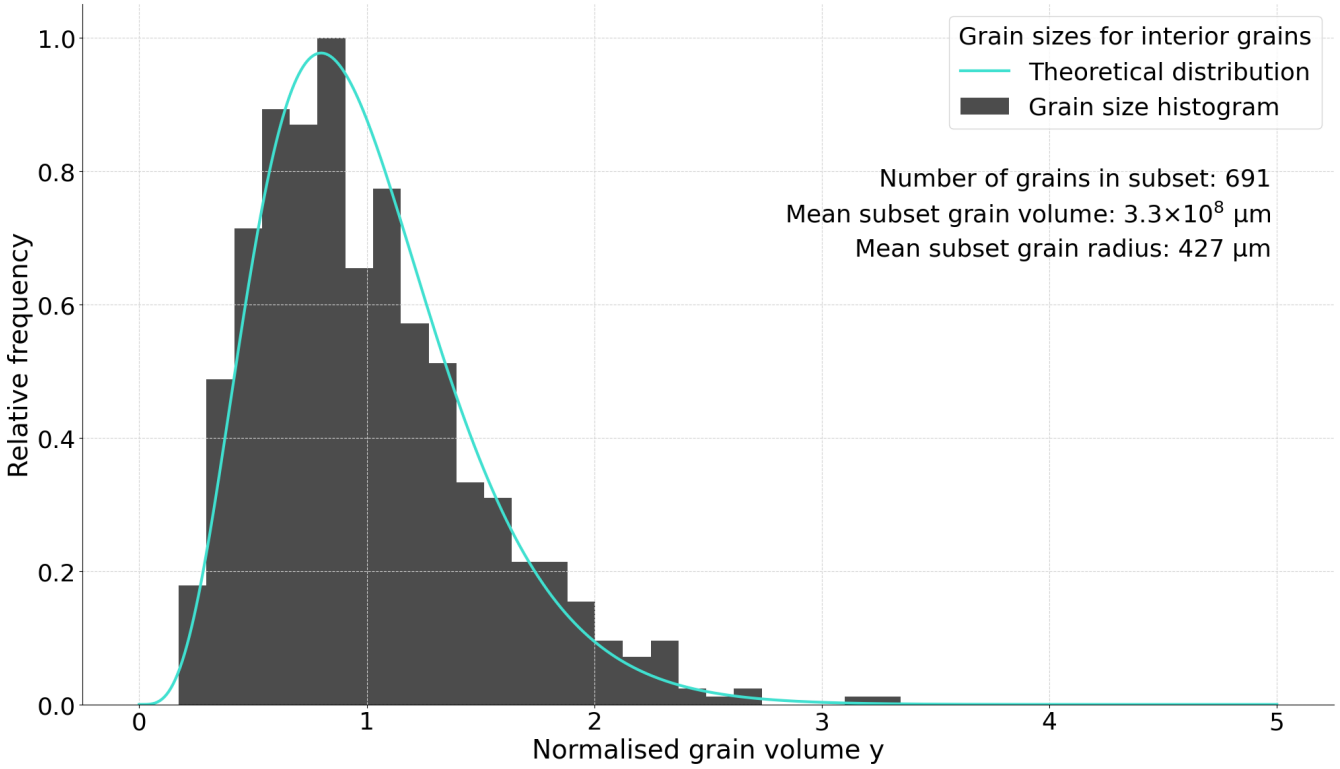

Figure S14. Grain volume distribution for the subset of grains fully contained within the same space as data plotted in Fig. S13.

Verification that modelled ice samples have a suitable grain volume distribution therefore can come from comparison with figures S13 and S14. To further verify these distributions, techniques such as that used for analysing high-resolution microstructure data (Binder et al., 2013) could also be applied to estimate grain volumes.

References

Binder, T., Garbe, C., Wagenbach, D., Freitag, J., and Kipfstuhl, S.: Extraction and parametrization of grain boundary networks in glacier ice, using a dedicated method of automatic image analysis, J. Microsc., 250, 130–141, https://doi.org/https://doi.org/10.1111/jmi.12029, 2013.

Ferenc, J.-S. and Néda, S.: On the size distribution of Poisson Voronoi cells, Physica A: Statistical Mechanics and its Applications, 385, 518–526, https://doi.org/https://doi.org/10.1016/j.physa.2007.07.063, 2007.

Quey, R., Dawson, P., and Barbe, F.: Large-scale 3D random polycrystals for the finite element method: Generation, meshing and remeshing, Computer Methods in Applied Mechanics and Engineering, 200, 1729–1745, https://doi.org/https://doi.org/10.1016/j.cma.2011.01.002, 2011.